CHAPTER VII
HYDROGEN PRODUCTION OVER Au-LOADED MESOPOROUS-ASSEMBLED $SrTiO_3$ NANOCRYSTAL PHOTOCATALYST: EFFECTS OF MOLECCULAR STRUCTURE AND CHEMICAL PROPERTIES OF HOLE SCAVENGERS

Abstract

The hydrogen production via the photocatalytic water splitting under UV irradiation using different compounds as hole scavengers (including methanol, formic acid, acetic acid, propanoic acid, hydrochloric acid, and sulfuric acid) under a low concentration range (< 8 vol.%) was investigated over the 1 wt.% Au-loaded mesoporous-assembled $SrTiO_3$ nanocrystal photocatalyst. The results indicated that the hydrogen production efficiency greatly depended on the molecular structure and chemical properties, and concentration of the hole scavengers. Formic acid, which is the smallest and completely-dissociated water-soluble carboxylic acid, exhibited the highest hydrogen production enhancement ability. The 2.5 vol.% aqueous formic acid solution system provided the highest photocatalytic hydrogen production rate.

7.1 Introduction

One of the major disadvantages of hydrogen production via the photocatalytic water splitting over most of the semiconductor photocatalysts is its relatively low efficiency, which is limited by three main causes, including the recombination reaction between photo-generated electrons and holes, the backward reaction between hydrogen and oxygen to reproduce water [1,2], and the limited light harvesting ability of photocatalysts [3-5]. An effective technique to retard the rate of the recombination reaction between photo-generated electrons and holes is the loading of noble and transition metal [6-9] or metal oxide [10-12] cocatalysts on the photocatalyst surface since the loaded metal or metal oxide cocatalyst particles can facilitate the interfacial electron transfer to the adsorbed protons and

To be published in Energy Conversion and Management, 52 (2011) 2256-2261

subsequently increase the proton reduction rate, thereby decreasing the possibility of the recombination reaction. The recombination reaction between the photo-generated electrons and holes can be also retarded by an addition of various hole scavengers, due to their ability to react with the photo-generated holes [12-13]. Moreover, a hole scavenger can react irreversibly with oxygen to suppress the backward reaction between hydrogen and oxygen [14], resulting in increasing the hydrogen production rate.

A variety of organic compounds, such as alcohols [2,6-9], organic acids [2,15], and aromatic compounds [16,17], can be efficiently used as the hole scavengers in the hydrogen production via the photocatalytic water splitting. The photocatalytic hydrogen production over a Pt-loaded $SrTiO_3$ photocatalyst suspended in ethylene diamine tetraacetic acid (EDTA), triethanolamine (TEOA), or $H_2PO_2^-$ solution was also investigated [18]. The results showed that $H_2PO_2^-$ was more effective in enhancing hydrogen production rate than EDTA and TEOA. This is in contrast to the use of TiO_2 as the photocatalyst, where EDTA was more effective than TEOA and $H_2PO_2^-$ [19]. It has been reported that the use of various alcohols as the hole scavengers exhibited different effects on the photocatalytic hydrogen production over different photocatalysts [20]. For instance, the hydrogen production efficiency over a Pt-loaded TiO_2 photocatalyst induced by alcohol-type hole scavengers decreased in the following order: ethanol > methanol > 1-propanol > 1-butanol. This is in contrast to the hydrogen production efficiency over a Pt-loaded $KCa_2Nb_3O_{10}$ photocatalyst, where the efficiency decreased in the following order: methanol > ethanol > 1-propanol > 1-butanol. Therefore, it can be concluded that the aid of hole scavengers to enhance the hydrogen production efficiency of the photocatalytic water splitting system is unclear and still in the research stage. Besides, the fundamental research is still needed in order to gain more basic knowledge, especially the role of hole scavengers to enhance the photocatalytic hydrogen production efficiency, and also in order to achieve the real-application purpose for the hydrogen production from naturally abundant water and sunlight resources.

In our previous works [21,22], the photocatalytic water splitting for hydrogen production over the mesoporous-assembled $SrTiO_3$-based photocatalysts was investigated to determine the effects of type and concentration of some hole scavengers, operating conditions, and metal type and loading. The previous results showed that the hydrogen production enhancement ability by using alcohol-type hole scavengers depended on their molecular weight and size, which are directly relevant to the ability to donate electrons to scavenge the photo-generated holes. However, the effects of molecular structure and chemical properties of hole scavengers on the photocatalytic hydrogen production activity have been scarcely reported.

Hence, the objective of this present work was to profoundly investigate the effects of molecular structure and chemical properties of hole scavengers on the hydrogen production efficiency from the photocatalytic water splitting. The acidic compounds—i.e. small molecular weight carboxylic acids (formic acid, acetic acid, and propanoic acid) and strong mineral acids (HCl and H_2SO_4)—were selected due to their efficient ability to donate proton. Methanol, a very weakly acidic alcohol, which showed the highest hydrogen production enhancement ability in our previous work [21], was also selected as the comparative hole scavenger. The 1 wt.% Au-loaded mesoporous-assembled $SrTiO_3$ nanocrystal photocatalyst synthesized by a single-step sol-gel method, which exhibited the highest hydrogen production activity as compared to the other mesoporous-assembled $SrTiO_3$ photocatalysts loaded with different metals with various loading contents [22], was selected to use in this work.

7.2 Experimental

7.2.1 Materials

Strontium nitrate ($Sr(NO_3)_2$, Merck Co., Ltd.), tetraisopropyl orthotitanate (TIPT, Merck Co., Ltd.), acetylacetone (ACA, S.D. Fine-Chem Ltd.), laurylamine (LA, Merck Co., Ltd.), hydrochloric acid (HCl, 37% analytical grade, Labscan Asia Co., Ltd.), and anhydrous ethanol (EtOH, 99.5% purity, Italmar Co., Ltd.) were used as starting materials for the synthesis of the mesoporous-assembled $SrTiO_3$ nanocrystal photocatalyst. Hydrogen tetrachloroaurate (III) trihydrate ($HAuCl_4 \cdot 3H_2O$, 99.99%, Alfa Aesar) was used as the Au co-catalyst precursor.

Anhydrous methanol (MeOH, 99.8% purity, Labscan Asia Co., Ltd.), formic acid (HCOOH, analytical grade, Labscan Asia Co., Ltd.), acetic acid (CH_3COOH, analytical grade, Labscan Asia Co., Ltd.), propanoic acid (CH_3CH_2COOH, analytical grade, Labscan Asia Co., Ltd.), hydrochloric acid (HCl, 37% analytical grade, Labscan Asia Co., Ltd.), and sulfuric acid (H_2SO_4, 40% analytical grade, Labscan Asia Co., Ltd.) were used as the hole scavengers for the investigation of the hydrogen production via the photocatalytic water splitting.

7.2.2 Synthesis Procedure of Photocatalysts

The mesoporous-assembled $SrTiO_3$ nanocrystal photocatalyst with 1 wt.% Au loading was synthesized via a sol-gel process with the aid of a structure-directing surfactant [22]. An ACA/TIPT solution was prepared by adding 2.00 g of ACA to 5.68 g of TIPT to obtain an equimolar proportion. A laurylamine hydrochloride (LAHC) surfactant solution was prepared by dissolving 1.02 g of LA with an equimolar HCl (0.09 g) in 50 cm^3 of EtOH. These two solutions were mixed to obtain a LAHC-to-TIPT molar ratio of 0.25:1. Then, 4.23 g of $Sr(NO_3)_2$ was added to the LAHC solution while stirring continuously to obtain a clear solution containing a Sr-to-Ti molar ratio of 1:1. After that, a 0.07 g of $HAuCl_4{\cdot}3H_2O$ was added to this clear solution to achieve 1 wt.% Au loading via a so-called single-step sol-gel method [22]. Afterwards, the LAHC-$Sr(NO_3)_2$-$HAuCl_4{\cdot}3H_2O$ solution was slowly dropped into the ACA/TIPT solution while stirring continuously. Next, the resulting mixture was incubated at 80°C for 1 d to obtain a complete gel formation. The resulting gel was further dried at 80°C for 2 d. Finally, the dried gel was calcined at 700°C with a heating rate of 1°C min^{-1}, and after reaching 700°C, it was maintained for 4 h to completely remove the LAHC surfactant from the dried gel to yield the 1 wt.% Au-loaded mesoporous-assembled $SrTiO_3$ nanocrystal photocatalyst.

7.2.3 Photocatalyst Characterization Techniques

The actual Au loading on the synthesized 1 wt.% Au-loaded $SrTiO_3$ photocatalyst was analyzed by X-ray fluorescence spectroscopy (XRF, Phillip, WD-

XRF model PW-2400). The crystallinity and the purity of the synthesized photocatalyst were examined by X-ray diffraction (XRD, Rigaku, RINT-2100) with a rotating anode XRD generating monochromated CuK_{α} radiation using continuous scanning mode at a rate of 2°C min^{-1} and operating conditions of 40 kV and 40 mA. The $SrTiO_3$ crystallite size was calculated from the line broadening of the $SrTiO_3$ (110) diffraction peak by using the Debye-Scherrer formula [23,24]. The N_2 adsorption–desorption isotherms of the synthesized photocatalyst were obtained by using a N_2 adsorption–desorption apparatus (BEL Japan, BELSORP-18 PLUS) at a liquid N_2 temperature of -196°C. The specific surface area of the synthesized photocatalyst was determined by the Brunauer-Emmett-Teller (BET) approach, whereas its pore size distribution and mean pore size were determined by the Barrett-Joyner-Halenda (BJH) approach. The particle sizes of the $SrTiO_3$ and loaded Au were obtained by using a transmission electron microscope (TEM, JEOL, JEM-200CX) at an operating voltage of 200 kV.

7.2.4 Photocatalytic hydrogen production system

The photocatalytic hydrogen production activity of the synthesized 1 wt.% Au-loaded $SrTiO_3$ photocatalyst was investigated by using the rate of hydrogen production during a 5-h irradiation period as a process performance parameter. The photocatalytic experiments were performed in an outer-irradiation and air-tight Pyrex glass reactor with a total volume of 750 cm^3. The reaction temperature was controlled by using a water-cooling system. A set of 176 W Hg lamps (Phillip Co. Ltd.), which emitted light with a total irradiating intensity of 2.3 mW cm^{-2}, was employed as UV light source. In a typical experiment, a quantity of 0.2 g of the synthesized photocatalyst was suspended by using a magnetic stirrer in an aqueous solution containing different concentrations of each hole scavenger. In order to investigate the effects of molecular structure and chemical properties of the hole scavengers used in this present work on the hydrogen production activity, the concentration of each hole scavenger was controlled to be less than 8 vol.% (low concentration range) in order to eliminate the unavoidable disturbed hydrogen production from the hole scavenger molecules themselves at high concentrations

[21]. Prior to the reaction testing, the suspension was left in the dark while simultaneously being thoroughly deaerated by Ar gas bubbling for 20 min, and then the suspension was irradiated by turning on the lamps for 5 h. The solution volume was controlled at 200 cm^3, and the reaction temperature was controlled at 45°C, which was found to be the most suitable reaction temperature [21]. A gas sample in the headspace of the photocatalytic reactor was periodically withdrawn at 1 h intervals and analyzed for hydrogen concentration by using a gas chromatograph (Hayesep D100/120, PerkinElmer) equipped with a thermal conductivity detector (TCD). The control experiments using the studied synthesized photocatalyst showed no hydrogen production under the dark environment in the presence of any given hole scavengers.

7.3 Results and discussion

7.3.1 Photocatalyst Characterization Results

The actual Au loading of the 1 wt.% Au-loaded mesoporous-assembled $SrTiO_3$ photocatalyst was confirmed by the XRF result to be 0.98 wt.%, clearly indicating no loss of the loaded Au during the single-step sol-gel synthesis. Figure 7.1 shows the XRD pattern of the synthesized photocatalyst. The dominant peaks at 2θ of about 32.4, 39.9, 46.4, 57.8, 67.8, and 77.2° indicates the indices of (110), (111), (200), (211), (220), and (310) planes, respectively, of the crystalline perovskite $SrTiO_3$ phase with a cubic structure (JCPDS card No. 35-0734) [25], with high purity and high crystallinity. As shown in Figure 7.1, no peaks of Au were detected possibly because of the low Au loading and the well-dispersed Au nanoparticles throughout the $SrTiO_3$ matrix. The $SrTiO_3$ crystallite size calculated by the Debye-Scherrer formula was approximately 35 nm. Figure 2 depicts the TEM image of the synthesized photocatalyst, in which it can be clearly observed in the form of aggregated clusters comprising a number of $SrTiO_3$ nanoparticles.

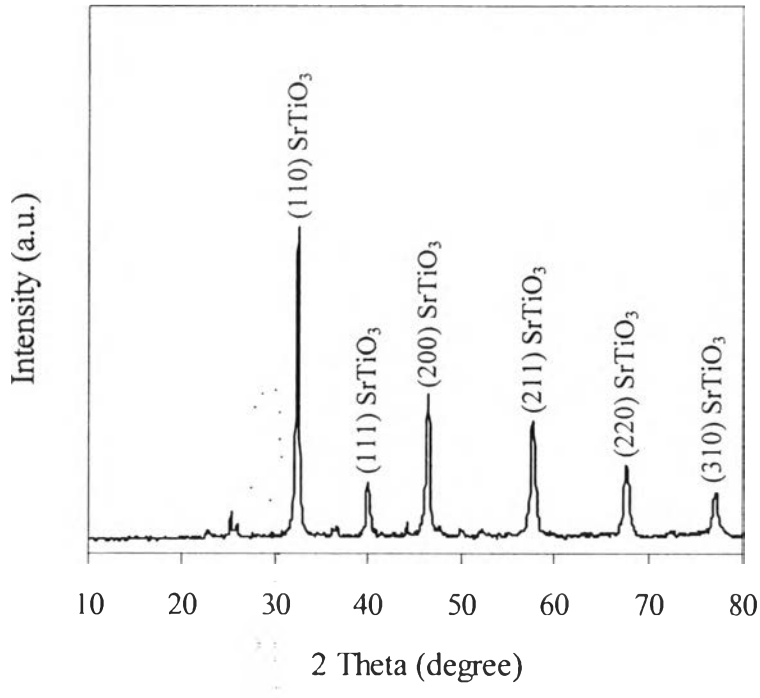

Figure 7.1 XRD pattern of the 1 wt.% Au-loaded mesoporous-assembled $SrTiO_3$ photocatalyst.

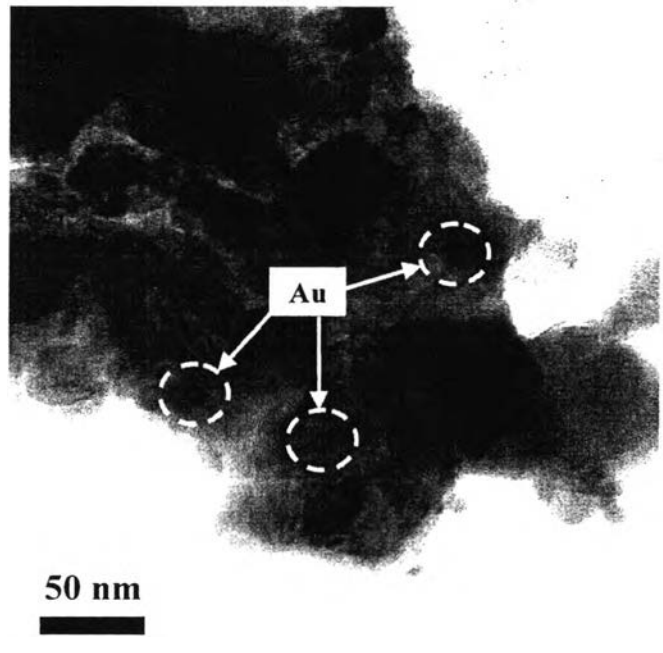

Figure 7.2 TEM image of the 1 wt.% Au-loaded mesoporous-assembled $SrTiO_3$ photocatalyst.

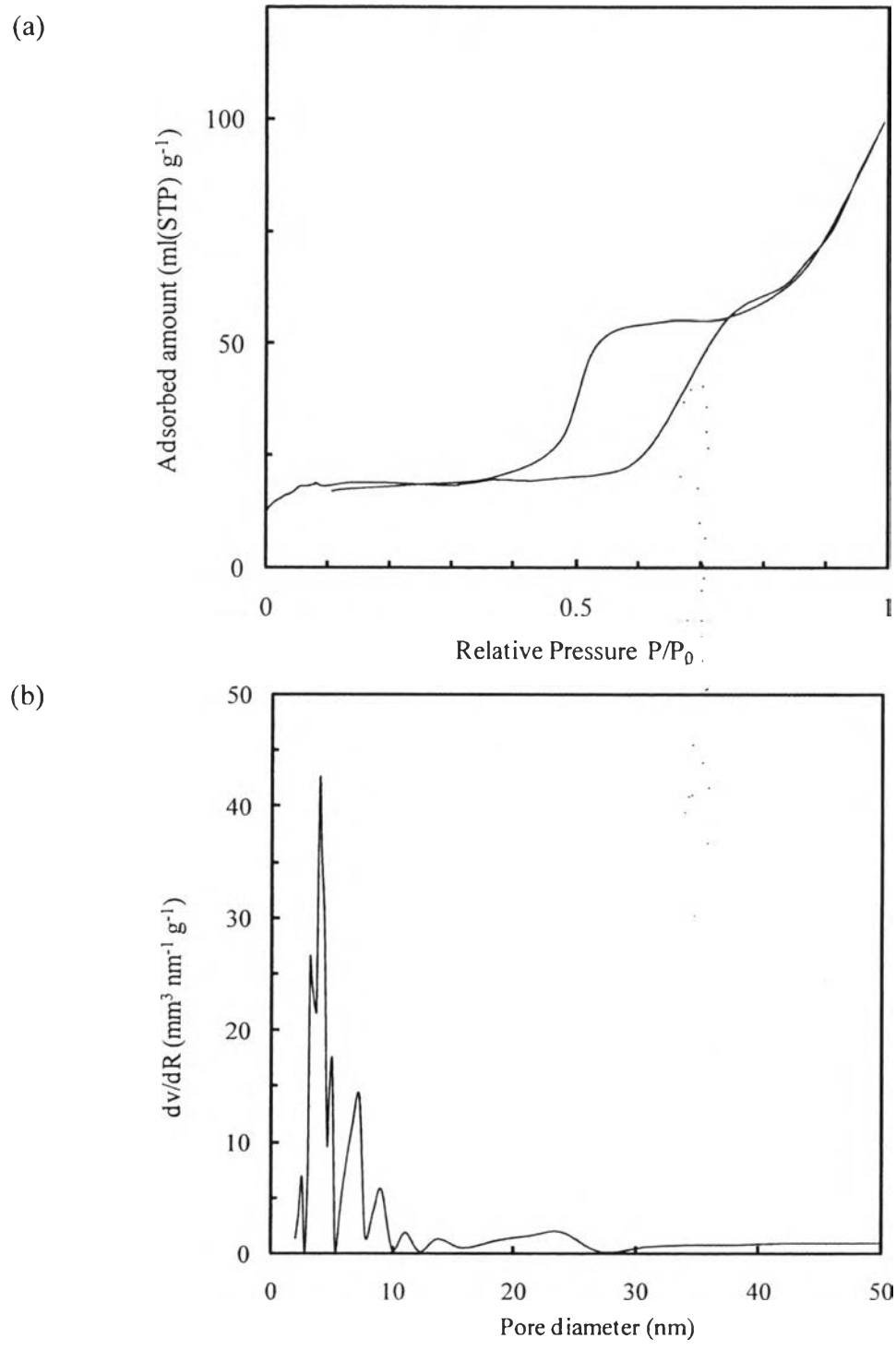

Figure 7.3 N_2 adsorption–desorption isotherms (a) and pore size distribution (b) of the 1 wt.% Au-loaded mesoporous-assembled $SrTiO_3$ photocatalyst.

The $SrTiO_3$ particle size obtained from the TEM analysis was in the approximate range of 25–40 nm, and it agrees well with its crystallite size calculated from the

XRD analysis, implying that each $SrTiO_3$ grain can be considered to be a single crystallite. In addition, from the TEM image (Figure 7.2), the Au particle size was found to be in the approximate range of 10–15 nm.

Figure 7.3 illustrates the N_2 adsorption–desorption isotherms and pore size distribution of the 1 wt.% Au-loaded mesoporous-assembled $SrTiO_3$ photocatalyst. As shown in Figure 3a, the isotherms belong to the IUPAC type IV pattern with an evident hysteresis loop, which is the principal characteristic of mesoporous materials [26]. The well-defined hysteresis loop with a sloping adsorption branch, a steep desorption branch, and a plateau at high relative pressures can be attributed to the H_2 type of the mesoporous materials. As can be seen from Figure 3b, a very narrow pore size distribution of the synthesized photocatalyst, which is entirely located in the mesoporous region (mesoporous size between 2 nm and 50 nm [26]), was clearly observed, indicating an advantage of the investigated sol-gel process in obtaining a good-quality product with a controlled porosity. The textural properties of the synthesized photocatalyst are as follows: a specific surface area of 8.64 $m^2\ g^{-1}$, a mean mesopore diameter of 4.4 nm, and a total pore volume of 74 $mm^3\ g^{-1}$.

7.3.2 Photocatalytic Hydrogen Production Results

The hydrogen production via the photocatalytic water splitting over the 1 wt.% Au-loaded mesoporous-assembled $SrTiO_3$ photocatalyst was investigated by using various hole scavengers: methanol, formic acid, acetic acid, propanoic acid, hydrochloric acid, and sulfuric acid. The hydrogen production rate during a 5 h irradiation period was used as the indicator of the photocatalytic hydrogen production efficiency. The effects of type and concentration of the hole scavengers on the specific hydrogen production rate are shown in Figure 7.4. The results show that the 1 wt.% Au-loaded mesoporous-assembled $SrTiO_3$ photocatalyst exhibited the photocatalytic activity for hydrogen production without the addition of any hole scavenger (i.e. in the pure water system) with the specific hydrogen production rate of 468 $\mu mol\ h^{-1}\ g_{cat}^{-1}$.

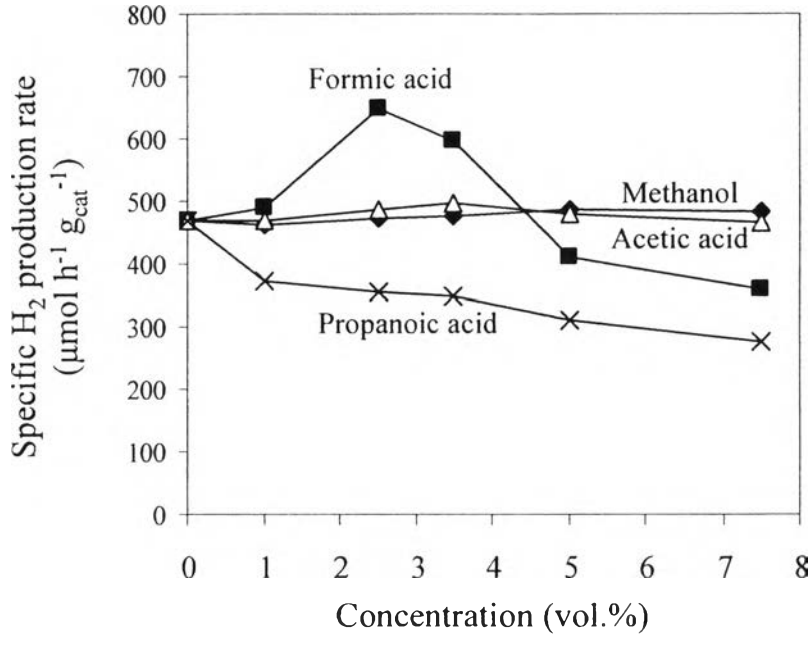

Figure 7.4 Dependence of specific H_2 production rate on type and concentration of the hole scavengers (system conditions: 5 h irradiation time, 200 cm^3 of aqueous hole scavenger solution, 0.2 g of 1 wt.% Au-loaded mesoporous-assembled $SrTiO_3$ photocatalyst, and 45°C reaction temperature).

According to the hydrogen production results from the water splitting reaction over the Au-loaded mesoporous-assembled $SrTiO_3$ photocatalyst with different hole scavengers (Figure 4), all of the investigated hole scavengers can be classified into three categories. The first category is the positive-effect hole scavenger, which increased the specific hydrogen production rate as compared to that of the pure water system, and formic acid is classified in this group. The increase in the formic acid concentration resulted in an increase in the specific hydrogen production rate, and the highest specific hydrogen production rate of 647 μmol h^{-1} g_{cat}^{-1} was obtained at a formic acid concentration of 2.5 vol.%. The further increase in the formic acid concentration beyond 2.5 vol.% led to the decrease in the specific hydrogen production rate. This observed negative effect is possibly due to the absorption of light by the hole scavenger molecule itself present in the solution

and/or adsorbed on the photocatalyst surface (possibly with several layers of adsorbed hole scavenger molecules at a higher concentration) instead of that by the photocatalyst to render the photoexcitation [27,28], leading to diminishing the hydrogen production from the photocatalytic water splitting.

The second category is the negative-effect hole scavenger, which decreased the specific hydrogen production rate as compared to that of the pure water system, and propanoic acid is classified in this group. The specific hydrogen production rate decreased significantly with increasing propanoic acid concentration throughout the investigated concentration range. The negative effect of propanoic acid is possibly because it has a large molecular size and is a non-dissociated water-soluble acid that can interact with H_2O molecule by an ionic force [29], resulting in its low accessibility to the active sites on the photocatalyst surface, as well as low mobility of H_2O to react with the photo-generated electrons and holes. These lead to the decrease in the hydrogen production efficiency, as compared to that of the pure H_2O system. The third category is the non-affecting hole scavenger, and methanol and acetic acid are classified in this group. The specific hydrogen production rate tended to remain almost unchanged with increasing methanol or acetic acid concentration, and no significant hydrogen production enhancement under the low concentration range (less than 8 vol.%) was observed in this present work. From our previous work [21], methanol was found to exhibit a significant hydrogen production enhancement when its concentration exceeded 20 vol.%.

From the hydrogen production results under the investigated low hole scavenger concentration range, the hydrogen production efficiency of each hole scavenger aqueous solution system is in the following order: formic acid > acetic acid ≅ methanol ≅ pure water > propanoic acid. The results suggest that the effect of hole scavenger on the hydrogen production efficiency greatly depends on its molecular structure, chemical properties, and concentration. The highest hydrogen production efficiency in the presence of formic acid as the hole scavenger is possibly due to its completely-dissociated water-soluble property ($HCOOH_{(aq)} \rightarrow HCOO^-_{(aq)} + H^+_{(aq)}$) (whereas acetic acid is a partially-dissociated water-soluble compound, but methanol and propanoic acid are the non-dissociated water-soluble compounds) [29],

and also due to its smaller molecular size (the molecular size of the investigated hole scavengers is in the following order: water < formic acid ≅ methanol < acetic acid < propanoic acid) [30]. The completely-dissociated water-soluble property of formic acid is possibly responsible for the ability enhancement of electron donation to scavenge the photo-generated holes and also for providing more quantity of protons in the solution to perform the proton reduction reaction for the hydrogen production. The smaller molecular size also possibly enhances the accessibility to active sites on the photocatalyst surface to scavenge the photo-generated holes.

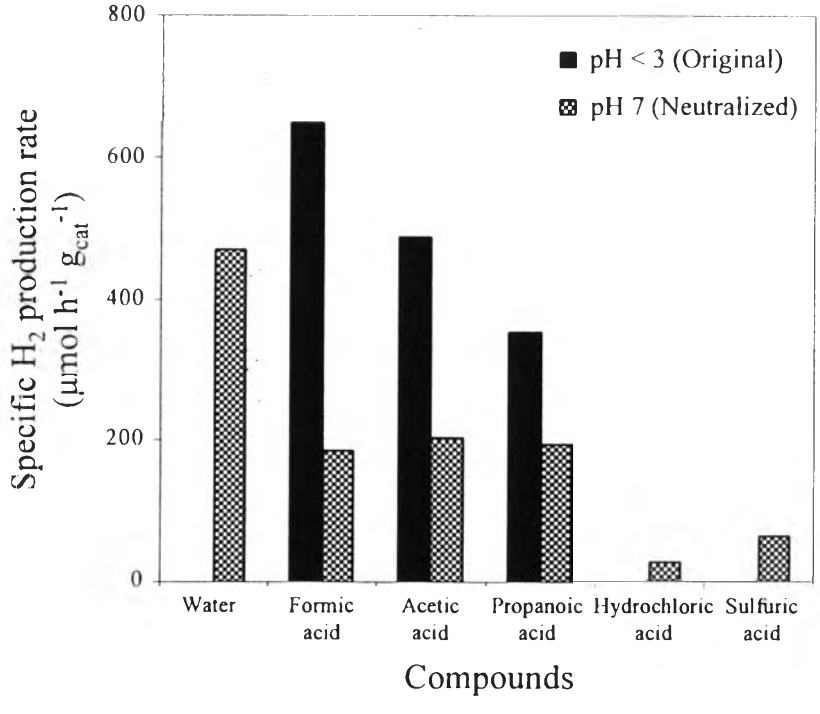

Figure 7.5 Dependence of specific H_2 production rate on initial solution pH value of the hole scavenger aqueous solution (system conditions: 5 h irradiation time, 200 cm^3 of aqueous hole scavenger solution, 2.5 vol.% of hole scavenger concentration, 0.2 g of 1 wt.% Au-loaded mesoporous-assembled $SrTiO_3$ photocatalyst, and 45°C reaction temperature).

The effect of initial solution pH of various molecular-structure hole scavengers on the hydrogen production efficiency was also investigated. Hydrochloric and sulfuric acids, which are strong mineral acids (the acidity of the investigated hole scavengers is in the following order: methanol < propanoic acid < acetic acid < formic acid < sulfuric acid < hydrochloric acid) [29], were comparatively used to investigate the effect of their hole-scavenging capability on the hydrogen production efficiency. The solution pH of each acidic hole scavenger aqueous system was also neutralized by using an aqueous NaOH solution before the hydrogen production activity was tested under the neutral condition as compared to that under the original acidic condition. The dependence of specific hydrogen production rate on the initial solution pH is shown in Figure 7.5. The results show that the hydrogen production from the formic acid, acetic acid, and propanoic acid aqueous solution systems were more favorable under the original acidic condition. Under the neutral condition, all of these systems showed a lower hydrogen production efficiency than that under the acidic condition. This is possibly because the anionic species of the investigated organic acids ($HCOO^-$, CH_3COO^-, and $CH_3CH_2COO^-$), which can irreversibly react with the photo-generated holes to provide H^+ and CO_2 under a normal condition, induce the salt formation when reacting with the Na^+, resulting in their lower ability to react with the photo-generated holes. The H^+ species from organic acid dissociation can also possibly react with the OH^- species (dissociated from NaOH added for the pH adjustment) to form H_2O, resulting in a lower amount of the H^+ species remaining in the solution. These result in a decrease in the probability of proton reduction reaction and thus a decrease in the hydrogen production efficiency. Moreover, since the point of zero charge (PZC) of $SrTiO_3$ photocatalyst in aqueous solution is about 8.5±0.3 [31], the lower solution pH (the original acidic condition) may induce a much more positively charged photocatalyst surface as compared to the neutralized solution pH (the neutral condition). This leads to a higher probability of the dissociated anionic species (i.e. $HCOO^-$, CH_3COO^-, and $CH_3CH_2COO^-$) to easily adsorb on the positively charged photocatalyst surface under the original acidic condition, causing an increased hole-scavenging capability and subsequently an enhanced hydrogen production efficiency. In the case of the hydrochloric and sulfuric acid aqueous solution systems

under the original acidic condition, no hydrogen production was observed, whereas under the neutral condition, both systems provided the hydrogen production (Figure 5). However, their hydrogen production efficiencies were comparatively low as compared to the other investigated organic hole scavengers, and even much lower than that of the pure water system. This clearly verifies the negative effect of salt formation (electrolyte effect) on the hydrogen production efficiency.

Table 7.1 Comparative results of specific H_2 production rate from the photocatalytic water splitting over various $SrTiO_3$-based photocatalysts

Photocatalyst	Hole scavenger	Reaction conditions (amount of photocatalyst and reactant solution)	Light source	Irradiation type	Specific H_2 production rate (μmol h^{-1} g_{cat}^{-1})	Reference
1 wt.% Au-loaded mesoporous-assembled $SrTiO_3$	CHOOH	0.2 g of photocatalyst, 200 ml of 2.5 vol.% aqueous CHOOH solution	176 W Hg lamp	Side (lateral) irradiation	647	This present work
0.03 mol% La-doped 0.2 wt.% CoO/$SrTiO_3$, with H_2 reduction at 773 K	Na_2CO_3	0.1 g of photocatalyst, 800 ml of deionized water containing Na_2CO_3	400 W high pressure Hg lamp	Side (lateral) irradiation	280	[32]
1 % Rh-doped 0.1 wt.% Pt-loaded $SrTiO_3$	MeOH	0.3 g of photocatalyst, 150 ml of 10 vol.% aqueous MeOH solution	300 W Xe lamp with cutoff filter ($\lambda > 440$ nm)	Top irradiation	117	[33]
4 mol% Cr-, 4 mol% Ta-doped 1 wt.% Pt-loaded $SrTiO_3$, with H_2 reduction at 773 K	MeOH	1 g of photocatalyst, 310 ml of 6.5 vol.% aqueous MeOH solution	300 W Xe lamp with cutoff filter ($\lambda > 440$ nm)	Not indicated	70	[9]
Hollow SiO_2-covered Pt-loaded $SrTiO_3$	-	0.05 g of photocatalyst, 150 ml of pure water	1 kW ultrahigh-pressure Hg arc lamp ($\lambda > 290$ nm)	Top irradiation	29	[34]
Pt-loaded $SrTiO_3$	-	0.05 g of photocatalyst, 150 ml of pure water	1 kW ultrahigh-pressure Hg arc lamp ($\lambda > 290$ nm)	Top irradiation	12.4	[34]

In order to evaluate the photocatalytic hydrogen production efficiency of the synthesized 1 wt.% Au-loaded mesoporous-assembled $SrTiO_3$ photocatalyst from the 2.5 vol.% aqueous formic acid solution (the best reaction solution in this present work) with some other published works from literature, the specific hydrogen production rates over various $SrTiO_3$-based photocatalysts and their corresponding photocatalytic reaction conditions and system configurations are comparatively summarized in Table 7.1. It should be noted that even though it is quite problematic to compare the photocatalytic activities obtained from different reaction conditions and system configurations (e.g. different photocatalyst amounts, different reaction solution volumes, different photocatalytic reactor configurations, different light source types and intensities, etc.), the hydrogen production efficiency in terms of specific hydrogen production rate (i.e. the hydrogen production rate per a constant one gram of photocatalyst used) can be sufficiently employed for such comparison purpose. Interestingly, it can be seen from Table 7.1 that the 1 wt.% Au-loaded mesoporous-assembled $SrTiO_3$ photocatalyst exhibited extraordinarily high hydrogen production efficiency from the 2.5 vol.% aqueous formic acid solution in this present work, as compared to the other published works. This comparison substantiates that the investigated photocatalyst possesses an outstanding photocatalytic property for water splitting when it is applied with a suitable hole scavenger system. Hence, it can be concluded that both the photocatalyst and hole scavenger significantly affect the hydrogen production efficiency via the photocatalytic water splitting.

7.4 Conclusions

The hydrogen production efficiency via the photocatalytic water splitting over the 1 wt.% Au-loaded mesoporous-assembled $SrTiO_3$ nanocrystal photocatalyst under the UV irradiation was found to depend on the molecular structure and chemical properties, and concentration of the investigated hole scavengers (under the low concentration range of less than 8 vol.%). From the results, the important properties directly affecting the enhancement ability of the hole scavenger were molecular size, water-soluble property, and acidity. The small molecular size, the

completely-dissociated water-soluble characteristic, and the high acidity of formic acid were responsible for its highest photocatalytic hydrogen production enhancement as compared to the other investigated hole scavengers. The 2.5 vol.% aqueous formic acid solution system exhibited the highest specific hydrogen production rate of 647 μmol h^{-1} g_{cat}^{-1} under the studied conditions.

7.5 Acknowledgments

The Commission on Higher Education, Ministry of Education, Thailand, is acknowledged for providing a Ph.D. scholarship (a Project on Faculty Development in Shortage Area Scholarship) to the first author. This work was also supported by the Research Grant for Mid-Career University Faculty (RMU) co-funded by the Thailand Research Fund (TRF); the Commission on Higher Education, Thailand; and Chulalongkorn University, Thailand. The authors would also like to thank the Sustainable Petroleum and Petrochemicals Research Unit, Center for Petroleum, Petrochemicals, and Advanced Materials, Chulalongkorn University, Thailand; and the Petrochemical and Environmental Catalysis Research Unit, Ratchadapisek Somphot Endowment Fund, Chulalongkorn University, Thailand.

7.6 References

1. M. Ni, M.K.H. Leung, D.Y.C. Leung, K. Sumathy, A review and recent developments in photocatalytic water-splitting using TiO_2 for hydrogen production, Renew. Sust. Energ. Rev. 11 (2007) 401-425.
2. A. Patsoura, D.I. Kondarides, X.E. Verykios, Photocatalytic degradation of organic pollutants with simultaneous production of hydrogen, Catal. Today 124 (2007) 94-102.
3. S. Hotchandani, P.V. Kamat, Charge-transfer processes in coupled semiconductor systems: photochemistry and photoelectrochemistry of the colloidal CdS-ZnO system, J. Phys. Chem. 96 (1992) 6834-6839
4. T. Sreethawong, C. Junbua, S. Chavadej, Photocatalytic H_2 production from water splitting under visible light irradiation using Eosin Y-sensitized mesoporous-assembled Pt/TiO_2 nanocrystal photocatalyst, J. Power Sources 190 (2009) 513-524.
5. M. Anpo, Preparation, characterization, and reactivities of high functional titanium oxide-based photocatalysts able to operate under UV-visible light irradiation: Approaches in realizing high efficiency in the use of visible light, Bull. Chem. Soc. Jpn. 77 (2004) 1427-1442.
6. T. Sreethawong, S. Yoshikawa, Comparative investigation on photocatalytic hydrogen evolution over Cu-, Pd-, and Au-loaded mesoporous TiO_2 photocatalysts, Catal. Commun. 6 (2005) 661-668.
7. T. Sreethawong, S. Yoshikawa, Enhanced photocatalytic hydrogen evolution over Pt supported on mesoporous TiO_2 prepared by single-step sol–gel process with surfactant template, Int. J. Hydrogen Energ. 31 (2006) 786-796.
8. T. Sreethawong, S. Laehsalee, S. Chavadej, Use of Pt/N-doped mesoporous-assembled nanocrystalline TiO_2 for photocatalytic H_2 production under visible light irradiation, Catal. Commun. 10 (2009) 538-543.
9. T. Ishii, H. Kato, A. Kudo, H_2 evolution from an aqueous methanol solution on $SrTiO_3$ photocatalysts codoped with chromium and tantalum ions under visible light irradiation, J. Photochem. Photobiol. A: Chem. 163 (2004) 181-186.

10. T. Sreethawong, Y. Suzuki, S. Yoshikawa, Photocatalytic evolution of hydrogen over mesoporous TiO_2 supported NiO photocatalyst prepared by single-step sol–gel process with surfactant template, Int. J. Hydrogen Energ. 30 (2005) 1053-1062.
11. T. Sreethawong, S. Ngamsinlapasathian, Y. Suzuki, S. Yoshikawa, Nanocrystalline mesoporous Ta_2O_5-based photocatalysts prepared by surfactant-assisted templating sol-gel process for photocatalytic H_2 evolution, J. Mol. Catal. A: Chem. 235 (2005)1-11.
12. H. Kato, A. Kudo, Photocatalytic water splitting into H_2 and O_2 over various tantalate photocatalysts, Catal. Today 78 (2003) 561-569.
13. S. Boumaza, R. Bouarab, M. Trari, A. Bouguelia, Hydrogen photo-evolution over the spinel $CuCr_2O_4$, Energ. Convers. Manage. 50 (2009) 62-68.
14. K. Sayama, H. Arakawa, Solar hydrogen production: significant effect of Na_2CO_3 addition on water splitting using simple oxide semiconductor photocatalysts, Catal. Surv. Jpn. 4 (2000) 75-80.
15. I.P. Pozdnyakov, Yu.A. Sosedova, V.F. Plyusnin, E.M. Glebov, V.P. Grivin, D.Yu. Vorobyev, N.M. Bazhin, Photodegradation of organic pollutants in aqueous solutions caused by $Fe(OH)^{2+}$ aqueous solution photolysis: evidence of OH radical formation, Int. J. Photoenerg. 6 (2004) 89-93.
16. K. Hashimoto, T. Kawai, T. Sakata, Photocatalytic reactions of hydrocarbons and fossil fuels with water: hydrogen production and oxidation, J. Phys. Chem. 88 (1984) 4083-4088.
17. J.R. Bolton, Solar photoproduction of hydrogen: a review, Sol. Energ. 57 (1996) 37-50.
18. M. Avudaithai, T.R.N. Kutty, Ultrafine powders of $SrTiO_3$ prepared by hydrothermal method and their photocatalytic activity, Mater. Res. Bull. 22 (1987) 641-650.
19. T.R.N. Kutty, M. Avudaithai, Sacrificial photolysis of water on TiO_2 fine powders prepared by the hydrothermal method, Mater. Res. Bull. 23 (1988) 725-734.
20. T. Takata, A. Tanaka, M. Hara, J.N. Kondo, K. Domen, Recent progess of photocatalysts for overall water splitting, Catal. Today 44 (1998) 17-26.

21. T. Puangpetch, T. Sreethawong, S. Yoshikawa, S. Chavadej, Hydrogen production from photocatalytic water splitting over mesoporous-assembled $SrTiO_3$ nanocrystal-based photocatalysts, J. Mol. Catal. A: Chem. 312 (2009) 97-106.
22. T. Puangpetch, T. Sreethawong, S. Chavadej, Hydrogen production over metal-loaded mesoporous-assembled $SrTiO_3$ nanocrystal photocatalysts: effects of metal type and loading, Int. J. Hydrogen Energ. 35 (2010) 6531-6540.
23. B.D. Cullity, Elements of X-ray Diffraction, Addison-Wesley Publishing Co., Reading, MA, 1978.
24. T. Puangpetch, T. Sreethawong, S. Yoshikawa, S. Chavadej, Synthesis and photocatalytic activity in methyl orange degradation of mesoporous-assembled $SrTiO_3$ nanocrystals prepared by sol-gel method with the aid of structure-directing surfactant, J. Mol. Catal. A: Chem. 287 (2008) 70-79.
25. J.V. Smith, X-ray Powder Data File, American Society for Testing Materials, New York, 1960.
26. F. Rouquerol, J. Rouquerol, K. Sing, Adsorption by Powders and Porous Solids: Principles, Methodology and Applications, Academic Press, San Diego, 1999.
27. I.K. Konstantinou, T.A. Albanis, TiO_2-assisted photocatalytic degradation of azo dyes in aqueous solution: kinetic and mechanistic investigations: A review, Appl. Catal. B: Environ. 49 (2004) 1-14.
28. W.F. Yao, X.H. Xu, H. Wang, J.T. Zhou, X.N. Yang, Y. Zhang, S.X. Shang, B.B. Huang, Photocatalytic property of perovskite bismuth titanate, Appl. Catal. B: Environ. 52 (2004) 109-116.
29. R.T. Morrison, R.N. Boyd, Organic Chemistry, Allyn and Bacon Inc., New York, 1987.
30. D.W. Green, R.H. Perry, Perry's Chemical Engineers' Handbook, McGraw-Hill, New York, 1997.
31. H.B. Ortiz-Oliveros, E. Ordoñez-Regil, S.M. Fernández-Valverde, Sorption of uranium(VI) onto strontium titanate in medium, J. Radioanal. Nucl. Chem. 279 (2009) 601-610.

32. Y. Qin, G. Wang, Y. Wang, Study on the photocatalytic property of La-doped CoO/$SrTiO_3$ for water decomposition to hydrogen, Catal. Commun. 8 (2007) 926-930.

33. R. Konta, T. Ishii, H. Kato, A. Kudo, Photocatalytic activities of noble metal ion doped $SrTiO_3$ under visible light irradiation, J. Phys. Chem. B 108 (2004) 8992-8995.

34. S. Ikeda, K. Hirao, S. Ishino, M. Matsumura, B. Ohtani, Preparation of platinized strontium titanate covered with hollow silica and its activity for overall water splitting in a novel phase-boundary photocatalytic system, Catal. Today 117 (2006) 343-349.